MALAYSIAN JOURNAL OF MICROSCOPY

Journal homepage: https://malaysianjournalofmicroscopy.org

RESEARCH ARTICLE

ENHANCED PHOTODEGRADATION OF METHYL ORANGE VIA TiO_2/g-C_3N_4 PHOTOCATALYST UNDER LOW-INTENSITY UVC (9W) IRRADIATION

Muhammad Aqil Asyraaf Mohd Mahadi[1], Nurul Amirah Abdullah[1], Hamizah Mokhtar[1], Hartini Ahmad Rafaie[2], Sazlinda Kamaruzaman[3], Umar Kalmar Nizar[4], Zul Adlan Mohd Hir[1,*]

[1]Faculty of Applied Sciences, Universiti Teknologi MARA Pahang Branch, 26400 Bandar Tun Abdul Razak Jengka, Pahang, Malaysia.
[2]Centre of Foundation Studies, Universiti Teknologi MARA Selangor Branch, Dengkil Campus, 43800 Dengkil, Selangor, Malaysia.
[3]Department of Chemistry, Faculty of Science, Universiti Putra Malaysia, 43400 Serdang, Selangor, Malaysia.
[4]Chemistry Department, Universitas Negeri Padang, West Sumatra, Indonesia.

Abstract. Synthetic anionic azo dyes, such as methyl orange (MO), represent substantial environmental issues because of their persistence and toxicity in water ecosystems. The presence of this dye in water bodies tends to pose significant risks to human health and the ecological systems under long-term exposure. Previous research has shown that the synergistic heterojunction formation between TiO_2 and g-C_3N_4 may reduce electron-hole recombination rate and enable the material to absorb more light, due to its extended absorption range, hence, significantly improving photoactivity. Thus, in the present work, TiO_2/g-C_3N_4 composite photocatalysts were prepared via a facile mixing procedure, with varying g-C_3N_4 ratios. The photodegradation performance was evaluated against the MO dye under a very low UVC light intensity (9 W). The surface morphology, composition, functional groups, recombination behaviours and band gap energy were characterised using SEM-EDX, FTIR, PL and UV-Vis-NIR, respectively. The fabrication of TiO_2/g-C_3N_4 composites has resulted in a significant enhancement in the photodegradation performance of pure TiO_2 and g-C_3N_4. The TiO_2/g-C_3N_4 with a ratio of 0.5:0.15 (TG2) demonstrated a rapid removal efficiency (~72 %) within 180 min under normal conditions, which was 1.4 times higher than that of pure TiO_2. The enhanced photoactivities were attributed to the outstanding separation of charge carriers (e_{CB}^-/h_{VB}^+) as demonstrated by the band gap and photoluminescence spectra studies. The kinetic display pseudo-first-order kinetics with a rate constant of 7.3×10^{-3} min^{-1}. This work revealed that the TiO_2/g-C_3N_4 composite photocatalysts exhibit promising potential for degrading dye molecules via the heterojunction mechanism.

Keywords: Graphitic carbon nitride, methyl orange, photocatalysis, titanium dioxide, water remediation.

Article Info

Received 2 January 2026
Accepted 27 April 2026
Published 8 June 2026

***Corresponding author: zuladlan@uitm.edu.my**

ISSN: 1823-7010, eISSN: 2600-7444

1. INTRODUCTION

Water pollution by dyes has become a pressing environmental issue and requires an effective solution. Several industries, such as leather, paper, textiles and printing, often discharge untreated wastewater containing dyes and other organic substances into the water bodies, which may affect human health and aquatic biota [1]. Dye has a complex molecular structure, which contributes to stability, high toxicity and difficulty in degrading with conventional water treatment methods. Methyl orange (MO) is one of the well-known dyes and has been extensively used in pharmaceutical, food, textiles, paper and research laboratories [2]. Currently, heterogeneous semiconductor photocatalysis has emerged as one of the most promising methods for organic dye degradation due to low cost, simplicity and its ability to absorb light (photon) to produce *in situ* reactive species such as photogenerated holes (h_{vb}^{+}), superoxide radicals anions ($\bullet O_2^{-}$) and hydroxyl radicals ($\bullet OH$). These species can break down complex dye molecules into simpler, less harmful intermediates, which are eventually converted into carbon dioxide (CO_2) and water (H_2O). In this view, this method offers some advantages with high potential in exploiting the abundant solar light source to address current energy and environmental problems [3].

Among the variety of semiconductors under research, titanium dioxide (TiO_2) remains widely used as a photocatalyst due to its high photostability and photoactivity, low cost and non-toxicity. However, it has some drawbacks: its wide bandgap (about 3.2 eV) and it has a high rate of electron-hole recombination, which lowers its efficiency [4]. To overcome these limitations, scientists have employed various methods, such as doping, surface modification and heterojunction formation with other semiconductors [1,4]. Recently, graphitic carbon nitride (g-C_3N_4) appeared to be a promising candidate to form a heterojunction with TiO_2. This material is a metal-free, n-type polymeric semiconductor with a small bandgap of 2.7 eV that could provide a feasible support to improve charge carriers' separation [4]. Previous research has shown that the synergistic heterojunction formation between TiO_2 and g-C_3N_4 may reduce electron-hole recombination rate and enable the material to absorb more light, due to its extended absorption range, hence, significantly improving photoactivity.

Several studies show that the integration of TiO_2 and g-C_3N_4 exhibited superior performance as compared to either pure TiO_2 or g-C_3N_4. For example, Ren et al. [4] reported that g-C_3N_4/TiO_2 nanocomposites degraded orange II dye with efficiency three times better than its individual photocatalyst. Meanwhile, Wang et al. [5] investigated that TiO_2/g-C_3N_4 films perform well in low-light conditions, making them a viable material for low-energy applications. Other than that, scientists have also constructed carbon-modified TiO_2/C/g-C_3N_4 hybrids that exhibit improved adsorption and greater visible-light dye removal, owing to their larger surface area and enhanced charge transfer [6]. Other combinations, such as TiO_2-ZnO/g-C_3N_4, show that these materials have a variety of applications by producing hydrogen in addition to improving dye removal [7]. Furthermore, research shows that the presence of different reactive species varies depending on the light and catalyst utilised. This suggests that both the catalyst and the light source can be modified to match the band gap energy of the catalyst for intended uses to boost photocatalytic potential.

Therefore, in this work, TiO_2/g-C_3N_4 composite photocatalysts were constructed by a facile mixing method with the use of commercial TiO_2 and dicyanamide as the precursor for g-C_3N_4. The mass of g-C_3N_4 was varied accordingly to find the optimum interface between the two materials that allows for more efficient charge carriers' separation, as well as altering surface characteristics to improve photodegradation performance. The surface morphological features, compositions, functional groups, recombination behaviours and band gap energy were investigated by employing an energy dispersive X-ray analyser (SEM-EDX), Fourier Transform Infrared (FTIR), photoluminescence (PL) and UV-Vis NIR, respectively. The photodegradation performance and kinetics of the composites were assessed against methyl orange (MO) dye, assisted by UVC light intensity (9 W), within 180 min. It is expected that this study will offer valuable motivation for the construction of an effective heterojunction mechanism for the photocatalytic water remediation process.

2. MATERIALS AND METHODS

2.1 Chemicals and Materials

Commercial dicyanamide ($(NH_2)_2C=NH$, 99 %) and titanium dioxide (TiO_2, 99 %, anatase-dominant phase, 14027) were supplied by Sigma-Aldrich (Selangor, Malaysia), respectively. Methyl orange dye was obtained from Bendosen Laboratory Chemical (Selangor, Malaysia). All chemicals were utilised as procured, without any refining step. Deionised water was utilised throughout the entire experiment.

2.2 Synthesis of g-C_3N_4

Dicyandiamide (0.1 mol) was allowed to dissolve in deionised water (50 mL) for 60 min with continuous stirring. The solution was then dried in an oven at 80 °C overnight prior to calcination at 500 °C for 2 h at a rate of 5 °C min^{-1}. Next, the sample was collected and dispersed in deionised water before undergoing bath sonication for another 2 h to allow the exfoliation process to take place. Lastly, the light-yellow sample was dried in the oven at 100 °C overnight and kept for later use [8].

2.3 Construction of TiO_2/g-C_3N_4 Composite Photocatalyst

The TiO_2/g-C_3N_4 composite photocatalyst was constructed via a facile mixing method with a variable mass ratio. The facile mixing method was selected due to its simplicity, low cost and scalability, although it may result in weaker interfacial contact compared to in situ synthesis methods. In brief, 0.50 g of TiO_2 and 0.05 g of g-C_3N_4 were dispersed in deionised water (50 mL), then continuously stirred for 1 h at room temperature. The process was preceded by drying the slurry mixtures at 80 °C overnight. The sample was then collected and labelled as TG1. The synergistic effect of TiO_2 and g-C_3N_4 was studied by formulating two other ratios of TiO_2 to g-C3N4 (0.50:0.15, 0.50:0.25), which were prepared under the same conditions (Table 1). Pure TiO_2 and g-C_3N_4 were also utilised to examine the photocatalytic activity for comparison purposes [8].

Table 1: Preparation of different mass ratios of TiO_2 and g-C_3N_4

Mass of TiO_2 (g)	Mass of g-C_3N_4 (g)	Labelled as
0.50	-	TiO_2
-	0.50	g-C_3N_4
0.50	0.05	TG1
0.50	0.15	TG2
0.50	0.25	TG3

2.4 Characterisations

The morphology and composition of TiO_2/g-C_3N_4 composites were analysed by using a scanning electron microscope attached with an energy dispersive X-ray analyser (SEM-EDX, TESCAN VEGA3). The functional groups were determined using a Fourier Transform Infrared (FT-IR) spectrophotometer in the range of 450-4000 cm^{-1} using a PerkinElmer Spectrum 100 FT-IR spectrophotometer. The photoluminescence (PL, FP-8500, JASCO) spectra were captured on a 325 nm excitation wavelength for the recombination behaviour study. A UV-vis NIR spectrophotometer (UV-3101PC Shimadzu) was used to measure the energy gap of the prepared composites. It should be noted that X-ray diffraction (XRD), CHNS elemental analysis, X-ray Photoelectron Spectroscopy (XPS) and Brunauer–Emmett–Teller (BET) analyses were not performed due to instrumental limitations. Therefore, crystalline phase confirmation and surface area quantification are acknowledged as limitations of this study and will be addressed in future work.

2.5 Evaluation of Photocatalytic Testing and Kinetic Study

The photocatalytic testing was conducted using a 250 mL beaker. Initially, a beaker with unadjusted 100 mL of 10 mg L^{-1} MO aqueous solution (pH=5.8) was filled with 0.2 g of TiO_2/g-C_3N_4 composites. Then, the MO solution was left in the dark for half an hour to achieve the adsorption-desorption equilibrium. The solution was then exposed to a UVC lamp (λ = 254 nm, 9 W) for 180 min while being continuously stirred. A low-intensity UVC lamp (9 W) was selected to simulate energy-efficient conditions, while 180 min duration ensures sufficient interaction time for observable degradation. Samples of 5 mL were taken at regular intervals of 30 min (0–180 min) to assess the residual concentration using a UV-vis Spectrophotometer (PerkinElmer Lambda 35) at a maximum wavelength of 464 nm. The degradation percentage and amount of degraded was evaluated using equations (1) and (2), respectively [9].

$$\text{Degradation percentage (\%)} = \frac{(C_o - C_t)}{C_o} \times 100 \quad (1)$$

$$\text{Amount of degraded (mg/g)} = \frac{(C_o - C_t) \times \text{Volume}}{\text{mass of catalyst}} \quad (2)$$

The photodegradation rate was investigated by using the Langmuir–Hinshelwood (L–H) kinetic model. The linear form that follows can be utilised to represent the pseudo-first-order kinetic [10].

$$\ln\left(\frac{C_o}{C_t}\right) = k_1 t \quad (3)$$

where C_o and C_t are the initial concentration and concentration at predetermined time intervals (t), respectively, and k_1 is the pseudo-first-order rate constant.

3. RESULTS AND DISCUSSION

3.1 Surface Morphological, Composition and Functional Group Analyses

The surface morphological and compositional characteristics of all photocatalysts were investigated using SEM-EDX, and the results are depicted in Figure 1. The results show that pure TiO_2 consists of a rough and porous surface with a semi-spherical shape. While pure g-C_3N_4 exhibited dense and stacked structures prone to agglomeration because of the π-π interactions. For TG1 composite, a similar morphology to pure TiO_2 can be seen with less dense structures. Meanwhile, TG2 seemed to consist of dense structures with a rough and more porous surface, but with fewer aggregated particles. TG3 had a more packed surface and denser particles due to the presence of a higher content of g-C_3N_4. All the composites show more porous and heterogeneous morphologies, suggesting stronger interfacial interactions between TiO_2 and g-C_3N_4, which further improved the dispersion for high surface area and enhanced photoactivity. The mapping images display good and uniform dispersion of the elements (Ti, O, C and N), confirming the successful formation of heterojunction in TiO_2/g-C_3N_4 structures (Figure 1(f)(i-v)). The strong Ti (red) and O (green) signals correspond to the TiO_2 phase. The uniformly dispersed C (purple) and N (yellow) signals indicate that g-C_3N_4 is well incorporated into the composite. Accordingly, the sample contains Ti (41.01 %), O (43.25 %), C (9.96 %) and N (5.78 %), which aligns with the expected TiO_2 composition, and the presence of C and N elements confirms the presence of g-C_3N_4. The appearance of Au peaks is simply due to the sputter-coating applied before analysis.

Overall, the elements are dispersed uniformly across the sample. Although SEM analysis provides insight into surface morphology, higher-resolution techniques such as HRTEM and

quantitative surface analysis (BET) are required for more precise evaluation of porosity and interfacial structure. These are recommended for future investigations.

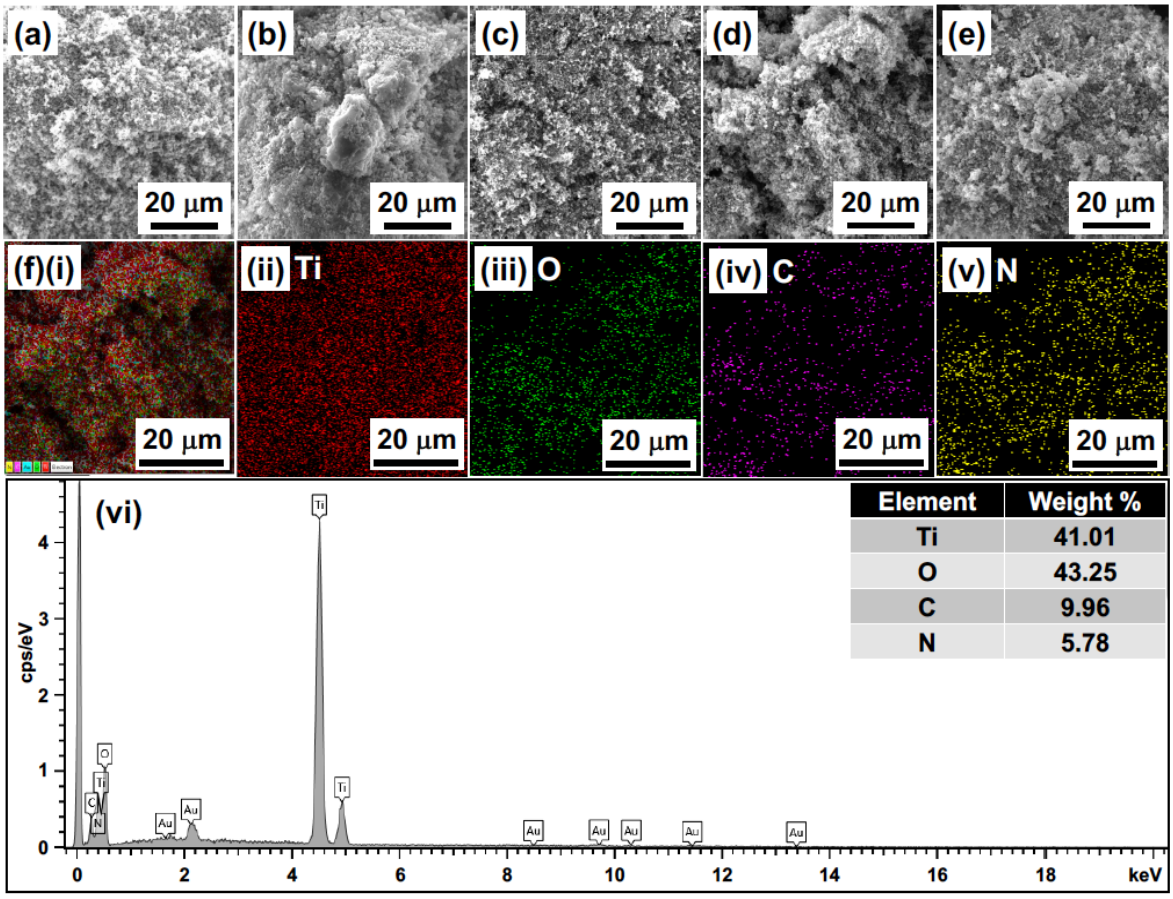

Figure 1: SEM images of (a) pure TiO_2, (b) pure g-C_3N_4, (c) TG1, (d) TG2, (e) TG3 composite photocatalysts and (f) (i-v) elemental mapping images of TG2

The FTIR spectra (Figure 2) of TG1 to TG3 display features of both TiO_2 and g-C_3N_4, confirming retention of their structures with interfacial interactions. Pure TiO_2 shows a broad 400-800 cm^{-1} band from Ti-O-Ti vibrations, while pure g-C_3N_4 exhibits N-H/O-H stretching (~3000-3500 cm^{-1}) [11], C-N and C=N stretching (1200-1650 cm^{-1}) and a triazine/heptazine ring breathing mode (~700-800 cm^{-1}) [12,13]. In the composite spectra (TG1, TG2, TG3), TG2 observes the retention of the Ti-O-Ti stretch (400-800 cm^{-1}), confirming that the TiO_2 framework remains intact. Simultaneously, signals in the range 1200-1650 cm^{-1} corresponding to C-N and C=N heterocycle vibrations persist in TG1 and TG3, although possibly with reduced intensity or slight shifts, indicating interaction or partial overlap between the phases. The triazine/heptazine mode near 810 cm^{-1} is retained, confirming preservation of g-C_3N_4 units. The diminished N-H/O-H stretching band suggests reduced free amine groups or less adsorbed moisture, consistent with TiO_2-g-C_3N_4 bonding reported in literature [12]. Qiu et al. [12] reported similar peak shifts and attenuation of the ~808 cm^{-1} mode in TiO_2/g-C_3N_4 composites, while Kocijan et al. [11] observed reduced O-H and Ti-OH bands after composite formation, attributed to calcination and loss of surface hydroxyl groups.

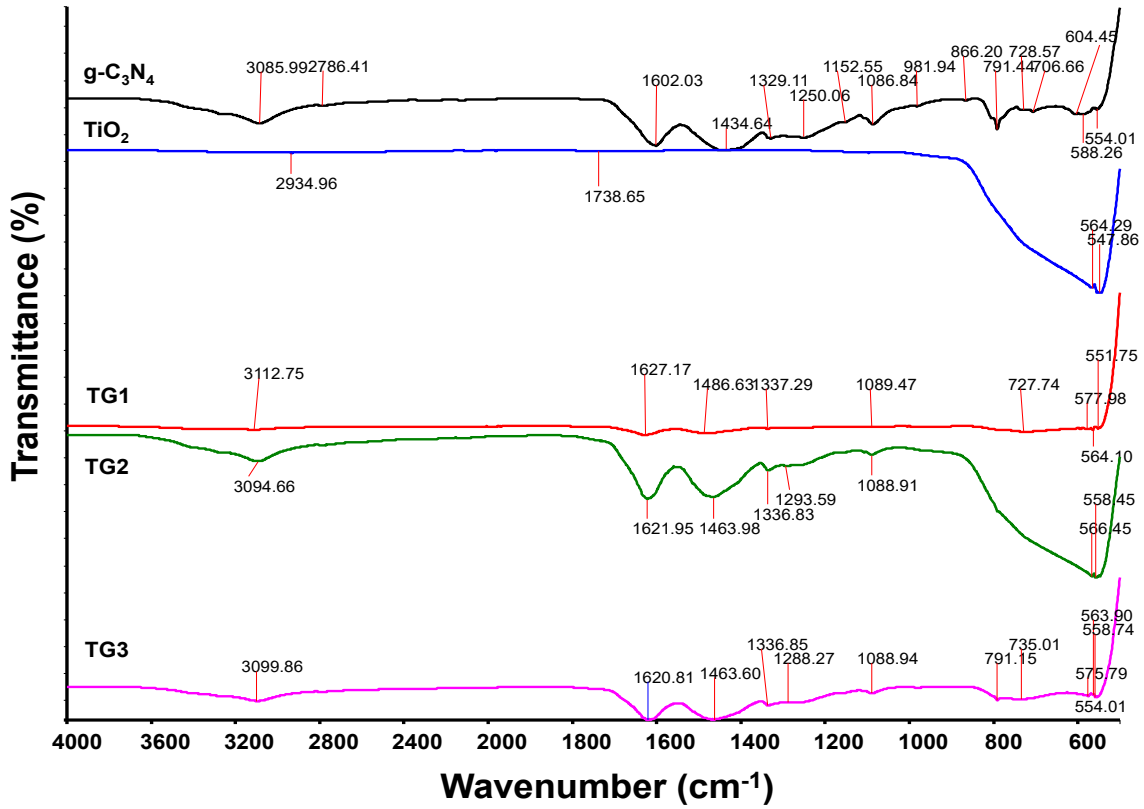

Figure 2: FTIR spectrum for pure TiO_2, pure g-C_3N_4, TG1, TG2 and TG3, respectively

3.2 Optical Response and Charge Recombination Analyses

The optical response of pure g-C_3N_4, pure TiO_2 and TiO_2/g-C_3N_4 composites was examined using UV-Vis NIR spectroscopy analysis (Figure 3). The results showed that pure g-C_3N_4 absorbed up to about 468 nm, while TiO_2 stopped around 400 nm. When combined, the composites shifted slightly to 406-420 nm, indicating that constructing a heterojunction provides new energy levels while narrowing the band gap [14]. The Tauc plot was used to analyse the correlation between $(\alpha h\upsilon)^{1/2}$ and photon energy ($h\upsilon$) (Figure 3(a)) for band gap energy estimation, assuming an indirect electronic transition. From the analysis, the estimated band gap energies of the composites were 3.05, 3.00 and 2.95 eV for TG1, TG2 and TG3, respectively. While pure g-C_3N_4 and TiO_2 exhibit band gaps of 2.65 and 3.10 eV, respectively. It can be observed that the band gap energies drop as the amount of g-C_3N_4 increases. This finding demonstrates that g-C_3N_4 introduces heterojunction sites, thereby lowering the band gap energy and making electron-hole pairs easier to form under light exposure. In comparison to pure TiO_2, the energy needed for the excitation of electrons from the valence band (VB) to the conduction band (CB) is reduced by g-C_3N_4 integration. In this view, the charge recombination rate can be lessened with an appropriate band alignment, resulting in improved high electron transfer and increased photocatalytic activity. A similar trend can also be seen in the previously reported study [8].

To verify the aforementioned inference, PL analysis was employed by examining the interfacial charge carrier separation and recombination behaviour of pure g-C_3N_4, pure TiO_2 and TiO_2/g-C_3N_4 composite photocatalysts stimulated at 325 nm (Figure 3(b)). The PL intensities of all composites reduced significantly in parallel with the increase in g-C_3N_4 content from 0.05 to 0.25 g. This phenomenon shows that g-C_3N_4 affects defect states and electronic structure, hence reducing charge recombination. Variations in PL intensity across varied TiO_2-to-g-C_3N_4 ratios suggest that the g-C_3N_4 presence affects charge carrier dynamics. Hypothetically, a high PL intensity indicates substantial electron-hole pair recombination, while a lower intensity indicates greater photoexcited electron-hole

pair separation efficiency, leading to enhanced photoactivity [15]. Moreover, a decrease in intensity compared to individual components indicates reduced electron-hole recombination, suggesting efficient charge separation typical of a Type-II structure. Overall, PL analysis showed enhanced photoexcited electron-hole separation efficiency in TiO_2/g-C_3N_4 composites photocatalysts.

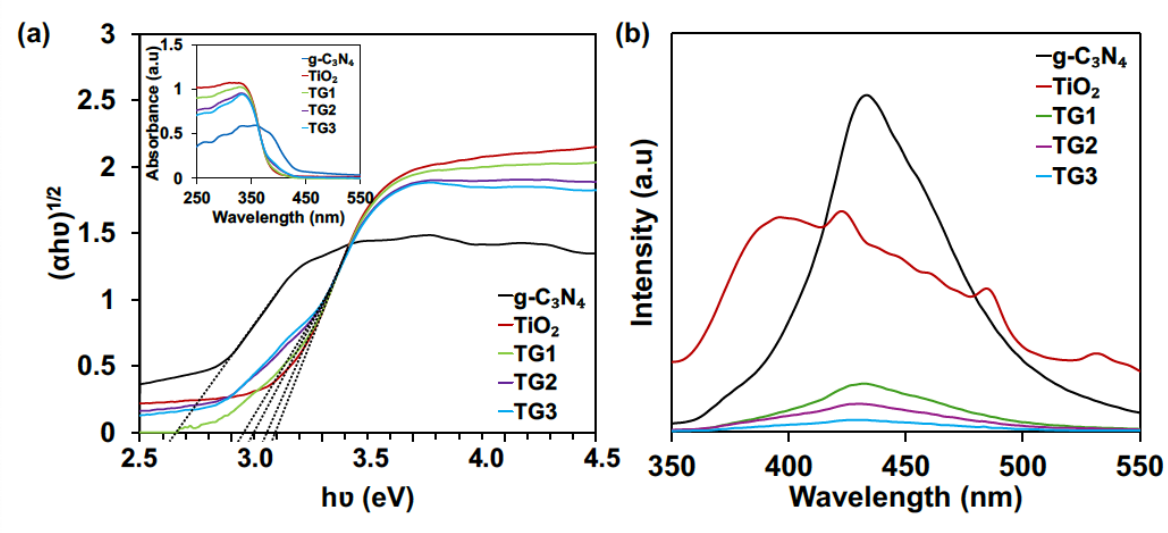

Figure 3: (a) Band gap energy (inset is absorbance spectra) and (b) PL spectra of pure g-C_3N_4, pure TiO_2 and TiO_2/g-C_3N_4 composite photocatalysts

3.3 Evaluation of Photocatalytic Testing and Kinetic Study

The photodegradation of MO by the prepared photocatalysts was monitored by UV-Vis Spectroscopy. The obtained results are presented in Figure 4 (a-d). In the control experiment, photolysis was negligible and all composites showed minimal adsorption in the first 30 min. Pure TiO_2 and g-C_3N_4 yielded removal percentages of 52.95 % and 24.02 %, respectively. While TG1, TG2 and TG3 significantly outperformed pure TiO_2 and g-C_3N_4, with TG2 achieving the highest percentage of ~72 % and rate constant of 7.30×10^{-3} min^{-1}. Overall, all composites successfully yielded higher degradation percentage and faster degradation rates than pure TiO_2 and g-C_3N_4, with TG2 showing the most balanced improvement in both kinetics and overall removal. From Figure 4 (a-b), all composites show steeper curves, indicating faster dye removal and higher degradation percentage. Linearised plots (Figure 4 (c-d)) yielded straight lines consistent with a pseudo-first-order kinetic model, amount of degraded, rate constant and degradation rates as tabulated in Table 2.

The superior activity of TG2 reflects an optimal TiO_2/g-C_3N_4 ratio that may enhance light absorption, suppress electron-hole recombination and degradation at active sites. However, further studies are needed to fully confirm the exact phenomenon occurring during degradation. In contrast, TiO_2 alone is limited by recombination, while g-C_3N_4 alone suffers from low quantum yield or weaker surface interactions. Comparisons to recent literature validate that the magnitudes seen in the data are plausible and competitive. For example, Lee et al. [16] achieved ~95.6 % MO degradation using TiO_2 quantum dots on g-C_3N_4, while Ma et al. [17] reported mesoporous TiO_2@g-C_3N_4 nanostructures with improved dye removal via larger surface area and stronger heterojunction contact. Together, these findings validate that heterostructure engineering enhances charge separation and surface reactivity, consistent with the improvements observed in all composite samples. Another study by Madima et al. [18] observed higher kinetics for TiO_2-g-C_3N_4 composites in degrading Rhodamine B dye.

It is important to note that the photocatalytic performance obtained in this study (72 % degradation) is lower than some advanced nanostructured systems reported in the literature, such as TiO_2 quantum dot-based heterojunctions. This difference is primarily attributed to the use of a facile

mixing method and operation under low-intensity UVC irradiation (9W) without extensive optimisation of parameters such as pH, temperature, or catalyst dosage. While such optimisation could further enhance performance, the present work emphasises energy-efficient operation and simple synthesis, offering a more practical and scalable approach for photocatalytic water treatment. Future studies will focus on parameter optimisation to further improve degradation efficiency.

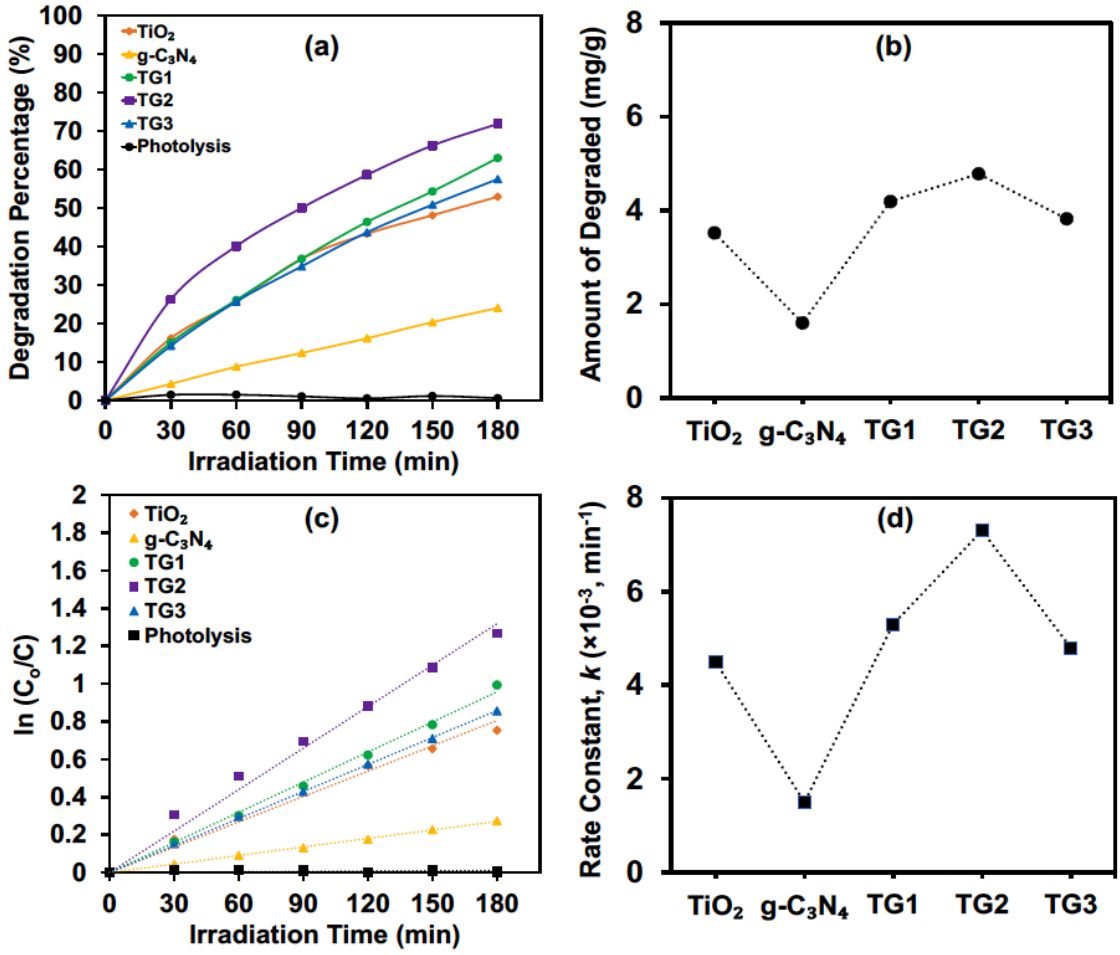

Figure 4: (a) Degradation percentages, (b) amount of MO degraded, (c) degradation kinetics and (d) rate constant for all photocatalysts

Table 2: Kinetics Constant of various photocatalysts for MO degradation

Photocatalyst	Degradation Percentage (%)	Amount of Degraded (mg g^{-1})	Rate Constant, k ($\times 10^{-3}$ min^{-1})	Rate (mg $L^{-1}min^{-1}$)	Correlation Factor, R^2
TiO_2	52.95	3.52	4.50	0.045	0.9942
g-C_3N_4	24.02	1.60	1.50	0.015	0.9997
TG1	62.99	4.19	5.30	0.053	0.9989
TG2	71.90	4.78	7.30	0.073	0.9963
TG3	57.53	3.82	4.80	0.048	0.9999

3.4 Photocatalytic Mechanism

The plausible mechanism for the photodegradation of MO dye using TiO_2/g-C_3N_4 composite photocatalyst is illustrated in Figure 5. The widely accepted mechanism for heterogeneous photocatalytic reactions is that the semiconductor absorbs light, which carries photons that have an equivalent or greater energy than the photocatalyst band gap, and then excites the electrons, generating photoexcited electrons (e_{CB}^-) at the conduction band (CB) and holes (h_{VB}^+) at the valence band (VB) [9,15]. In this case, both base photocatalyst components have the capability to absorb photons simultaneously due to the Type-II heterojunction formation. The band alignment and charge transfer mechanism are proposed based on UV-Vis NIR analysis. Through this mechanism, a better charge carrier separation can be achieved by transferring the electrons from the CB of g-C3N4 to the CB of TiO2 and holes vice versa. Moreover, the integration of these two materials could narrow the band gap and prolong the photocatalytic reactions under UVC irradiation, resulting in a synergistic photocatalytic effect. The reactive species, such as $\bullet O_2^-$, •OH and h_{VB}^+, were generated through a sequence of redox events involving electrons and adsorbed oxygen, as well as holes and adsorbed water, leading to the degradation of MO molecules. The application of UVC irradiation significantly increased the generation of •OH radicals by the decomposition of produced hydrogen peroxide (H_2O_2), as demonstrated in Equations (4-10), leading to a substantial proportion of MO degradation. The potential accumulation of electrons at the TiO_2 conduction band is mitigated by their rapid consumption through the reduction of dissolved oxygen to $\bullet O_2^-$ radicals, ensuring continuous charge transfer and maintaining reaction equilibrium. Unlike UVC irradiation, UVA and UVB irradiation cannot convert H_2O_2 into •OH radicals [19]. The findings show that a suitable amount of the counterpart photocatalyst could really boost the photocatalytic activity; however, excessive amounts are detrimental [20]. The photocatalytic degradation process proceeds through a sequence of redox reactions involving photogenerated electrons and holes, leading to the formation of reactive oxygen species (ROS). The stepwise reactions are described as follows:

$$TiO_2/g\text{-}C_3N_4 + h\nu \rightarrow e_{CB}^- + h_{VB}^+ \quad (4)$$

$$e_{CB}^- + O_2 \rightarrow \bullet O_2^- \quad (5)$$

$$h_{VB}^+ + H_2O \rightarrow \bullet OH + H^+ \quad (6)$$

$$\bullet O_2^- + H^+ \rightarrow \bullet OOH \quad (7)$$

$$\bullet OOH + H^+ \rightarrow H_2O_2 \quad (8)$$

$$H_2O_2 + e_{CB}^- \rightarrow \bullet OH + OH^- \quad (9)$$

$$\text{MO dye} + \bullet OH \rightarrow \text{Degradation products} \rightarrow CO_2 + H_2O \quad (10)$$

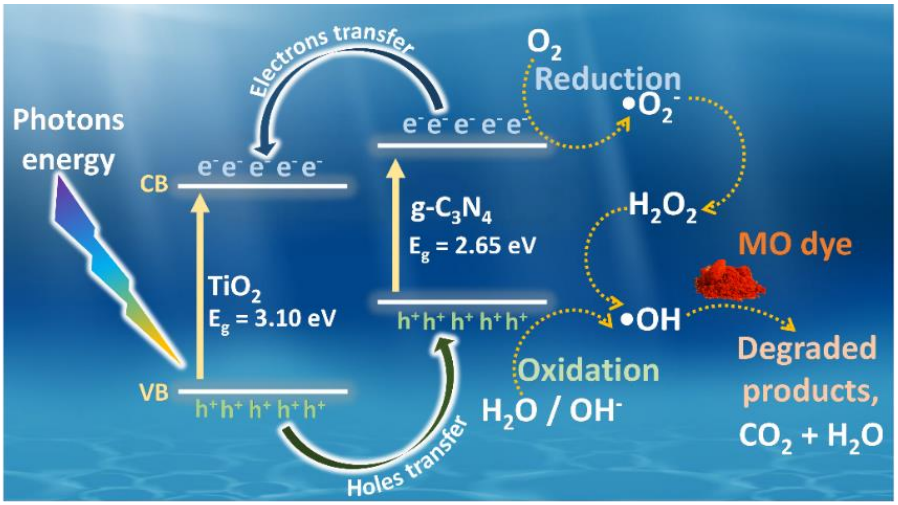

Figure 5: Plausible mechanism of MO degradation using TiO_2/g-C_3N_4 composite photocatalyst

4. CONCLUSION

In conclusion, this study demonstrates the facile fabrication and characterisation of TiO_2/g-C_3N_4 photocatalysts for MO degradation under low UVC light intensity. The morphological and structural characterisation using SEM and EDX-mapping confirmed the uniform distribution and dense morphology of the TiO_2/g-C_3N_4 particles, with g-C_3N_4 successfully integrated with TiO_2, as evidenced by the EDX spectra. The optical analyses via UV-Vis NIR indicate band gap narrowing and PL analysis demonstrated a substantial degree of effective charge separation in TiO_2/g-C_3N_4 composites via heterojunction formation. Optimizing TiO_2/g-C_3N_4 ratios improved activity, achieving 71.9 % degradation by using the TG2 catalyst. Kinetic analysis followed a pseudo-first-order model (k = 7.30 × 10^{-3}), with reactive species driving the dye degradation. Overall, TiO_2/g-C_3N_4 composites show strong potential as efficient photocatalysts for practical wastewater remediation. Despite promising results, limitations such as a lack of RAMAN, FESEM, CHNS, XPS, XRD, BET and scavenger studies highlight the need for further investigation. Future work should focus on advanced characterisation and optimisation under varying operational conditions. It should also be noted that the present study focuses on compositional optimisation rather than synthesis condition optimisation. The TiO_2/g-C_3N_4 composites were prepared under fixed conditions using a facile mixing method. Further optimisation of synthesis parameters, such as calcination temperature, mixing duration and interfacial engineering, is recommended for future studies to enhance photocatalytic performance.

Acknowledgements

The authors are grateful to the Ministry of Higher Education, Malaysia, under the Fundamental Research Grant Scheme (FRGS) (Project Number: FRGS/1/2024/STG05/UITM/02/12), UiTM Cawangan Pahang and Universiti Putra Malaysia for facilities to carry out the research work, management and technical support.

Author Contributions

All authors contribute towards data analysis, drafting and revising the paper.

Disclosure of Conflict of Interest

The authors declare there is no conflict of interest in this work.

Compliance with Ethical Standards

The work is compliant with ethical standards.

References

[1] Sewnet, A., Abebe, M., Asaithambi, P. & Alemayehu, E. (2022). Visible-light-driven g-C3N4/TiO2 based heterojunction nanocomposites for photocatalytic degradation of organic dyes in wastewater: a review. *Air, Soil and Water Research*. 15, 117862212211172.

[2] Guo, B., Uzzaman, M., Furukawa, M., Tateishi, I., Katsumata, H. & Kaneco, S. (2024). Photocatalytic purification of orange-ii-dye-polluted wastewater using TiO2-modified g-C3N4 composite. *Journal of Carbon Research*. 10(4), 103.

[3] Dai, J., Wu, Y., Yao, Y. & Zhang, B. (2025). ZnO/TiO2 photocatalysts for degradation of methyl orange by low-power irradiation. *Science Progress*. 108(1), 368504251322606.

[4] Ren, B., Wang, T., Qu, G., Deng, F., Liang, D., Yang, W. & Liu, M. (2018). In situ synthesis of g-C3N4/TiO2 heterojunction nanocomposites as a highly active photocatalyst for the degradation of Orange II under visible light irradiation. *Environmental Science and Pollution Research*. 25(9), 19122-19133.

[5] Wang, P., Guo, X., Rao, L., Wang, C., Guo, Y. & Zhang, L. (2018). A weak-light-responsive TiO2/g-C3N4 composite film: photocatalytic activity under low-intensity light irradiation. *Environmental Science and Pollution Research*. 25(20), 20206–20216.

[6] Khan, A., Jonathan, R., Rehman, S. U., Shoaib, M., Cao, F., Ali, S., Bououdina, M., Ismail, P. M., Wang, J., Abu-Farsakh, H., Liu, Y. & Jian, X. (2024). Ultra-fine carbon decorated TiO2/C/g-C3N4 hybrid for strong physical adsorption and efficient photodegradation of pollutants. *Arabian Journal of Chemistry*. 18(1), 106034.

[7] Liu, J., Gao, Y., Zhang, Z., Dang, R., Tiri, R. N. E. H., Bayat, R., Darabi, R. & Sen, F. (2023). Photocatalytic activity of TiO2-ZnO/g-C3N4 nanocomposites for methylene orange and Rhodamine B dyes removal from water and photocatalytic hydrogen generation. *Chemosphere*. 339, 139426.

[8] Izhar, N. I., Hir, Z. A. M., Rafaie, H. A. & Daud, S. (2024). Physicochemical characterization of ZnO/g-C3N4 for photo-removal of methyl orange under low uv-light intensity. *Malaysian Journal of Analytical Sciences.* 28(2), 365–375.

[9] Mukhair, H., Abdullah, A. H., Hir, Z. A. M., Osman, N. S., Zainal, Z. & Ngee, L. H. (2023). In-depth investigation on the photostability and charge separation mechanism of Ag3PO4/g-C3N4 photocatalyst towards very low visible light intensity. *Journal of Molecular Liquids*. 376, 121494.

[10] Bahrudin, N. (2022). Evaluation of degradation kinetic and photostability of immobilized TiO2/activated carbon bilayer photocatalyst for phenol removal. *Applied Surface Science Advances*. 7, 100208.

[11] Kocijan, M., Vukšić, M., Kurtjak, M., Ćurković, L., Vengust, D. & Podlogar, M. (2022). TiO2-based heterostructure containing g-C3N4 for an effective photocatalytic treatment of a textile dye. *Catalysts*. 12(12), 1554.

[12] Qiu, J., Feng, Y., Zhang, X., Zhang, X., Jia, M. & Yao, J. (2017). Facile stir-dried preparation of g-C3N4/TiO2 homogeneous composites with enhanced photocatalytic activity. *RSC Advances*. 7(18), 10668–10674.

[13] Negro, P., Cesano, F., Casassa, S. & Scarano, D. (2023). Combined DFT-D3 computational and experimental studies on g-C3N4: new insight into structure, optical, and vibrational properties. *Materials*. 16(10), 3644.

[14] Rafaie, H. A., Ramli, N. I. T., Khusaimi, Z., Sarjidan, M. A. M., Dulyaseree, P. & Hir, Z. A. M. (2023). Ag2CO3-based photocatalyst with enhanced photocatalytic activity for endocrine-disrupting chemicals degradation: a review. *Catalysts*. 13(3), 540.

[15] Syazwani, O. N., Hir, Z. A. M., Mukhair, H., Mastuli, M. S. & Abdullah, A. H. (2018). Designing visible-light-driven photocatalyst of Ag3PO4/CeO2 for enhanced photocatalytic activity under low light irradiation. *Journal of Materials Science Materials in Electronics*. 30(1), 415–423.

[16] Lee, J., Jeong, S., Son, Y. & Lee, S. (2023). Facile fabrication of TiO2 quantum dots-anchored g-C3N4 nanosheets as 0d/2d heterojunction nanocomposite for accelerating solar-driven photocatalysis. *Nanomaterials*, 13(9), 1565.

[17] Ma, L., Fang, Z., Duan, J., Li, J., Zhu, K., Jiang, Y., Ji, B. & Yang, Z. (2024). Mesoporous TiO2@g-C3N4 nanostructure-enhanced photocatalytic degradation of tetracycline under full-spectrum sunlight. *Molecules*. 29(24), 5981.

[18] Madima, N., Kefeni, K. K., Mishra, S. B. & Mishra, A. K. (2022). TiO2-modified g-C3N4 nanocomposite for photocatalytic degradation of organic dyes in aqueous solution. *Heliyon*. 8(9), e10683.

[19] Khataee, A. & Zarei, M. (2011). Photocatalysis of a dye solution using immobilized ZnO nanoparticles combined with photoelectrochemical process. *Desalination*. 273(2–3), 453–460.

[20] Rosman, S., Rafaie, H. A., Yahya, S. N. H., Kamil, S. A., Supardan, S. N., Mokhtar, H. & Hir, Z. A. M. (2025). Facile synthesis and structural characterization of chromium-doped zinc oxide photocatalysts for photo-removal of methylene blue under uv-light intensity irradiation. *Malaysian Journal of Chemistry*. 27(2). 64–74.